2010 American Control Conference
Marriott Waterfront, Baltimore, MD, USA
June 30-July 02, 2010

ThC18.4

Experimental evaluation of a nonlinear attitude observer based on image and inertial measurements

S. Brás, R. Cunha, J.F. Vasconcelos, C. Silvestre and P. Oliveira

Abstract— **This paper presents an experimentally tested solution to the problem of estimating the attitude of a rigid body using rate gyros and a pan and tilt camera. An exponential input-to-state stable pan and tilt control law is used to keep the visual features in the image plane. A multi-rate implementation of the nonlinear attitude observer that uses recent results in geometric numeric integration is proposed. Practical aspects, such as the computation of suitable observer feedback gains, are considered. Experimental results obtained with a high accuracy motion rate table demonstrate the high level of performance attained by the proposed solution.**

I. INTRODUCTION

Vision-based techniques can be seen as a reliable alternative to GPS based navigation for the operation of Unmanned Aerial Vehicles (UAVs) in indoor and urban environments. The literature on vision-based rigid-body stabilization and estimation addresses important problems such as i) keeping feature visibility along the system's trajectories for a large region of attraction [1] ii) guaranteeing convergence in the presence of camera parametric uncertainty and image measurement noise [2], iii) establishing observability conditions for attitude estimation [3]. The aim of this paper is the development and experimental evaluation of a nonlinear vision based observer to estimate the vehicle attitude relative to a set of feature points.

In many applications it is desired to design observers based only on the rigid body kinematics, which are an exact description of the physical quantities involved. In this approach, the attitude of the vehicle is propagated by integrating inertial sensor measurements [4], [5]. Research on the problem of deriving a stabilizing law for systems evolving on manifolds, where attitude is parameterized, can be found in [6], [7], and [8], which provide important guidelines for observer design and discuss the topological limitations to achieving global stabilization on the SO(3) manifold.

The development of numeric integration methods that preserve geometric properties evolving on Lie groups has witnessed in the last two decades a remarkable progress. These methods were originally proposed by Crouch and Grossman in [9]. In [10] the author constructs generalized Runge-Kutta methods where the computations are performed in the Lie algebra, which is a linear space. More recently, the work in [11] describes commutator-free Lie group methods to overcome some of the problems associated with the computation of commutators.

The authors are with the Institute for Systems and Robotics (ISR), Instituto Superior Técnico, Lisbon, Portugal. E-mails: {sbras, rita, jfvasconcelos, cjs, pjcro}@isr.ist.utl.pt
Tel: (+351) 21-8418054, Fax: (+351) 21-8418291.

The work of S. Brás and J.F. Vasconcelos was supported by PhD Student Scholarships from FCT POCTI programme, SFRH/BD/47456/200 and SFRH/BD/18954/2004, respectively.

In this work we consider the problem of estimating the attitude of a rigid body equipped with a triad of rate gyros and a pan and tilt camera. By exploiting directly sensor information, a stabilizing feedback law with exponential convergence to the origin of the estimation errors is proposed. As a second goal, we develop an active vision system targeted at keeping the features inside the image plane. For that purpose, an image-based control law for the camera pan and tilt angular rates is proposed.

To assess in practice the performance of the proposed observer, an experimental setup, comprising a MemSense nIMU and an AXIS 215 PTZ camera was assembled and mounted on a motion rate table that enables the acquisition of ground truth data. The Model 2103HT from Ideal Aerosmith [12] is a three-axis motion rate table that provides precise angular position and rate.

The paper is structured as follows. In Section II, the attitude estimation and the camera pan and tilt control problems are introduced. In Section III the attitude observer is presented, and its properties are highlighted. The camera pan and tilt controller is derived in Section IV. A low complexity discrete time implementation of the observer is proposed in Section V. The experimental setup is described in Section VI, and experimental results that illustrate the performance of the proposed solution are presented in Section VII. Finally, concluding remarks are given in Section VIII.

II. PROBLEM FORMULATION

Consider a rigid body equipped with a triad of rate gyros and a pan and tilt camera. Let $\{B\}$ be the frame attached to the rigid body, $\{L\}$ the local frame attached to the feature plane, and $\{C\}$ the camera frame with origin at the camera's center of projection with the z-axis aligned with the optical axis. The navigation problem illustrated in Fig. 1 can be summarized as the problem of estimating the attitude of a rigid body given by the rotation matrix from $\{L\}$ to $\{B\}$, denoted as ${}^L_B\mathbf{R}$, using images of a collection of feature points and angular velocity readings. An image-based controller for the camera pan and tilt angles that enforces feature visibility is also proposed.

A. Sensor Suite

The triad of rate gyros is assumed to be aligned with $\{B\}$ so that it provides measurements of the body angular velocity $\boldsymbol{\omega}_B$ corrupted by a constant bias term $\boldsymbol{\omega}_r = \boldsymbol{\omega}_B + \mathbf{b}_\omega$, $\dot{\mathbf{b}}_\omega = \mathbf{0}$.

As shown in Fig. 1, the camera can describe pan and tilt motions corresponding to the angles ψ and ϕ, respectively.

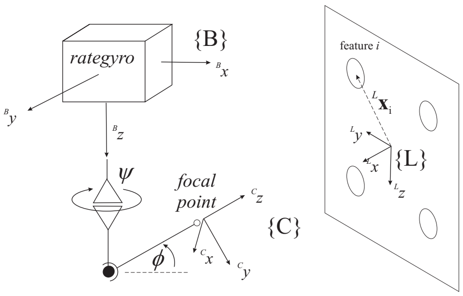

Fig. 1. Diagram of the experimental setup.

As such the rotation matrix from $\{C\}$ to $\{B\}$ is given by

$$\begin{aligned} {}^B_C\mathbf{R} &= \mathbf{R}_{\text{pan}}\mathbf{R}_{\text{tilt}}, \\ \mathbf{R}_{\text{pan}} = \mathbf{R}_z(\pi/2+\psi), &\quad \mathbf{R}_{\text{tilt}} = \mathbf{R}_x(\pi/2+\phi) \end{aligned} \tag{1}$$

where $\mathbf{R}_z(\cdot)$ and $\mathbf{R}_x(\cdot)$ denote rotation matrices about the z-axis and x-axis, respectively.

For simplicity of notation, we denote the configuration of $\{C\}$ with respect to $\{L\}$ by $(\mathcal{R}, \mathbf{p}) \in \mathrm{SE}(3)$, where $\mathcal{R} = {}^L_C\mathbf{R}$ is the rotation matrix from $\{C\}$ to $\{L\}$ and $\mathbf{p}$ the position of the origin of $\{L\}$ with respect to $\{C\}$. The observed scene consists of four points whose coordinates in $\{L\}$ are denoted by ${}^L\mathbf{x}_i \in \mathbb{R}^3$, $i \in \{1,\ldots,4\}$. Without loss of generality, the origin of $\{L\}$ is assumed to coincide with the centroid of the feature points so that $\sum_{i=1}^4 {}^L\mathbf{x}_i = 0$. The 3-D coordinates of the features points expressed in $\{C\}$ can be written as $\mathbf{q}_i = \mathcal{R}^T {}^L\mathbf{x}_i + \mathbf{p}$, $i \in \{1,\ldots,4\}$ and, using the perspective camera model [2], the 2-D image coordinates of those points $\mathbf{y}_i \in \mathbb{R}^2$ can be written as

$$\begin{bmatrix} \mathbf{y}_i \\ 1 \end{bmatrix} = \delta_i \mathbf{A}\mathbf{q}_i, \tag{2}$$

where $\mathbf{A} \in \mathbb{R}^{3\times 3}$ is the camera calibration matrix assumed to be known and δ_i is an unknown scalar encoding depth information and given by $\delta_i = (\mathbf{e}_3^T\mathbf{q}_i)^{-1}$, $\mathbf{e}_3 = [0\ 0\ 1]^T$.

B. Attitude kinematics

The camera frame attitude kinematics can be described by

$$\dot{\mathcal{R}} = \mathcal{R}[\boldsymbol{\omega}]_\times, \tag{3}$$

where once again for simplicity of notation $\boldsymbol{\omega} \in \mathbb{R}^3$ denotes the camera angular velocity and $[\mathbf{w}]_\times$ is the skew symmetric matrix defined such that $[\mathbf{w}]_\times\mathbf{y} = \mathbf{w}\times\mathbf{v}$, with $\mathbf{w},\mathbf{v} \in \mathbb{R}^3$. Taking the time derivative of (1), straightforward computations show that $\boldsymbol{\omega}$ can be written as

$$\boldsymbol{\omega} = {}^C_B\mathbf{R}\boldsymbol{\omega}_B + \mathbf{R}_{\text{tilt}}^T[\dot{\phi}\ 0\ \dot{\psi}]^T, \tag{4}$$

where $\dot{\psi}$ and $\dot{\phi}$ are the time derivatives of the camera pan and tilt angles, respectively. Assuming that we solve the attitude estimation problem for $\mathcal{R}$ and that the camera pan and tilt angles are known, we can readily obtain the attitude of the rigid body ${}^L_B\mathbf{R} = \mathcal{R}{}^C_B\mathbf{R}$ as proposed.

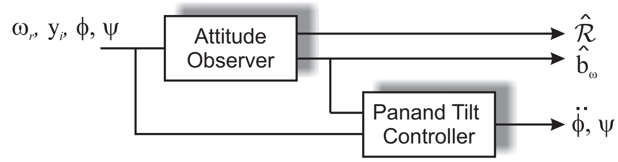

Fig. 2. Block diagram of the attitude observer and camera controller. The quantities $\hat{\mathcal{R}}$ and $\hat{\mathbf{b}}_\omega$ are, respectively, the attitude and angular rate bias estimates.

C. Problem Summary

The estimation problem addressed in this paper can be stated as follows.

Problem 1: Consider the attitude kinematic model described by (3). Design a dynamic observer for $\mathcal{R}$ based on $\boldsymbol{\omega}_r$ and $\mathbf{y}_i$, $i = \{1,\ldots,4\}$, with the largest possible basin of attraction.

To develop an active vision system using the camera pan and tilt degrees of freedom, we consider the following problem.

Problem 2: Let $\bar{\mathbf{y}}$ be the image of the features' centroid given by $[\bar{\mathbf{y}}^T\ 1]^T = \bar{\delta}\mathbf{A}\mathbf{p}$, $\quad \bar{\delta} = (\mathbf{e}_3^T\mathbf{p})^{-1}$. Design a control law for $\dot{\psi}$ and $\dot{\phi}$ based on $\boldsymbol{\omega}_r$ and $\mathbf{y}_i$, $i \in \{1,\ldots,4\}$, such that $\bar{\mathbf{y}}$ approaches the center of the image plane.

Figure 2 depicts the cascaded composition of the system, where the angular rate bias estimate is fed into the pan and tilt controller.

III. ATTITUDE OBSERVER

In the following, we propose a solution to Problem 1 that builds on results presented in [4], where a nonlinear position and attitude observer based on landmark measurements and biased velocity measurements was shown to provide exponential convergence to the origin for the position, attitude, and bias errors. The proposed observer is designed to match the rigid body attitude kinematics taking the form

$$\dot{\hat{\mathcal{R}}} = \hat{\mathcal{R}}[\hat{\boldsymbol{\omega}}]_\times, \tag{5}$$

where $\hat{\mathcal{R}}$ is the estimated camera attitude and $\hat{\boldsymbol{\omega}}$ is the feedback term designed to compensate for the estimation errors.

Some rotational degrees of freedom are unobservable in the case features are all collinear as discussed in [4] and references therein. The following necessary condition for attitude estimation is assumed.

Assumption 1: The features are not all collinear.

We will consider a feedback law for $\hat{\boldsymbol{\omega}}$ that uses measurements of the form

$$\mathbf{U} = \mathcal{R}^T[{}^L\mathbf{u}_1\ \ldots {}^L\mathbf{u}_5] \in \mathbb{R}^{3\times 5}, \tag{6}$$

where ${}^L\mathbf{u}_i \in \mathbb{R}^3$ are time-invariant in the local frame $\{L\}$. To obtain these vector readings from the image coordinates $\mathbf{y}_i$, we explore the geometry of planar scenes. For that purpose, we introduce the matrices

$$\mathbf{X} = \begin{bmatrix} {}^L\mathbf{x}_1 & \cdots & {}^L\mathbf{x}_4 \end{bmatrix}, \quad \mathbf{Y} = \begin{bmatrix} \mathbf{y}_1 & \cdots & \mathbf{y}_4 \\ 1 & \cdots & 1 \end{bmatrix},$$

where ${}^L\mathbf{x}_i$ are the 3-D coordinates of the feature points expressed in $\{L\}$ and $\mathbf{y}_i$ the corresponding 2-D image coordinates. We can now state the following lemma.

Lemma 1: Let $\boldsymbol{\sigma} = [\sigma_1\ \sigma_2\ \sigma_3\ \sigma_4]^T \in \mathbb{R}^4 \setminus \{0\}$ and $\boldsymbol{\rho} = [\rho_1\ \rho_2\ \rho_3\ \rho_4]^T \in \mathbb{R}^4 \setminus \{0\}$ be such that $\mathbf{Y}\boldsymbol{\sigma} = 0$, $\mathbf{X}\boldsymbol{\rho} = 0$, and $\mathbf{1}^T\boldsymbol{\rho} = 0$, where $\mathbf{1} = [1\ 1\ 1\ 1]^T$. Consider that the features verify Assumption 1 and that the camera configuration is such that the image is not degenerated (neither a point nor a line). Then, the depth variables δ_i can be written as $\delta_i = \alpha\frac{\rho_i}{\sigma_i}$,where $\alpha \in \mathbb{R}$, $\rho_i \neq 0$, and $\sigma_i \neq 0$ for $i \in \{1, 2, 3, 4\}$.

Proof: See [13]. ■

Writing (2) in matrix form and using Lemma 1, we have $\mathbf{Y} = \mathbf{A}(\mathcal{R}^T\mathbf{X} - \mathbf{p}\mathbf{1}^T)\alpha\mathbf{D}_\sigma^{-1}\mathbf{D}_\rho$, where $\mathbf{D}_\rho = \mathrm{diag}(\boldsymbol{\rho})$. From the feature centroid constraint $\mathbf{X}\mathbf{1} = 0$, it follows that $\alpha\mathcal{R}^T\mathbf{X} = \mathbf{A}^{-1}\mathbf{Y}\mathbf{D}_\rho^{-1}\mathbf{D}_\sigma(\mathbf{I} - \frac{1}{4}\mathbf{1}\mathbf{1}^T)$, which takes the form of (6) up to a scale factor. We can use the properties of the rotation matrix and the positive depth constraint $\delta_i > 0$ to obtain the normalized vector readings

$$
{}^C\bar{\mathbf{x}}_i = \mathcal{R}^T\frac{{}^L\mathbf{x}_i}{\|{}^L\mathbf{x}_i\|} = \mathrm{sign}(\alpha)\frac{\alpha\mathcal{R}^{T\,L}\mathbf{x}_i}{\|\alpha\mathcal{R}^{T\,L}\mathbf{x}_i\|}. \tag{7}
$$

where $\mathrm{sign}(\alpha) = \mathrm{sign}\left(\frac{\rho_i}{\sigma_i}\right)$. Finally, we define the matrix $\mathbf{U}$ using linear combinations of (7) so that $\mathbf{U} = {}^C\bar{\mathbf{X}}\mathbf{A}_X$, where $\mathbf{A}_X \in \mathbb{R}^{5\times5}$ is nonsingular and ${}^C\bar{\mathbf{X}} = [{}^C\bar{\mathbf{x}}_1,\ \ldots,\ {}^C\bar{\mathbf{x}}_4,\ {}^C\bar{\mathbf{x}}_i \times {}^C\bar{\mathbf{x}}_j]$ for any linearly independent ${}^C\bar{\mathbf{x}}_i$ and ${}^C\bar{\mathbf{x}}_j$.

The directionality associated with the features positions is made uniform by defining transformation $\mathbf{A}_X$ such that $\mathbf{U}\mathbf{U}^T = \mathbf{I}$. The desired $\mathbf{A}_X$ exists if Assumption 1 is satisfied [4].

Let the bias in angular velocity measurements be constant, i.e. $\dot{\mathbf{b}}_\omega = \mathbf{0}$, and consider the Lyapunov function

$$
V = \frac{\|\tilde{\mathcal{R}} - \mathbf{I}\|^2}{2} + \frac{1}{2k_{b_\omega}}\|\tilde{\mathbf{b}}_\omega\|^2,
$$

where $k_{b_\omega} > 0$, $\tilde{\mathbf{b}}_\omega := \hat{\mathbf{b}}_\omega - \mathbf{b}_\omega$, and $\hat{\mathbf{b}}_\omega$ is the estimated bias in angular velocity measurements. Its time derivative is given by

$$
\dot{V} = \mathbf{s}_\omega^T(\hat{\boldsymbol{\omega}} - {}^C_B\mathbf{R}\boldsymbol{\omega}) + \frac{1}{k_{b_\omega}}\dot{\hat{\mathbf{b}}}_\omega^T\tilde{\mathbf{b}}_\omega, \tag{8}
$$

where $\mathbf{s}_\omega = \mathcal{R}^T[\tilde{\mathcal{R}} - \tilde{\mathcal{R}}^T]_\otimes$, and $[\cdot]_\otimes$ is the unskew operator, such that, $[[\mathbf{a}]_\times]_\otimes = \mathbf{a}$, $\mathbf{a} \in \mathbb{R}^3$. The feedback term $\mathbf{s}_\omega$ can be expressed as an explicit function of the sensor readings [4, Theorem 8].

$$
\mathbf{s}_\omega = \sum_{i=1}^{5}(\hat{\mathcal{R}}^{T\,L}\bar{\mathbf{X}}\mathbf{A}_X\mathbf{e}_i) \times (\mathbf{U}\mathbf{e}_i)
$$

Consider the attitude feedback law

$$
\begin{aligned}
\hat{\boldsymbol{\omega}} &= {}^C_B\mathbf{R}(\boldsymbol{\omega}_r - \hat{\mathbf{b}}_\omega + \mathbf{R}_{\text{pan}}^T[\dot{\phi}\ 0\ \dot{\psi}]^T) - k_\omega\mathbf{s}_\omega \\
&= {}^C_B\mathbf{R}(\boldsymbol{\omega} - \tilde{\mathbf{b}}_\omega + \mathbf{R}_{\text{pan}}^T[\dot{\phi}\ 0\ \dot{\psi}]^T) - k_\omega\mathbf{s}_\omega,
\end{aligned} \tag{9}
$$

where $k_\omega > 0$. Applying the feedback law (9) to the Lyapunov function (8) and defining

$$
\dot{\hat{\mathbf{b}}}_\omega := k_{b_\omega}{}^B_C\mathbf{R}\mathbf{s}_\omega, \tag{10}
$$

the Lyapunov function derivative is given by $\dot{V} = -k_\omega\|\mathbf{s}_\omega\|^2$.

Considering the feedback law (9) and the differential equation (10), the closed loop attitude error dynamics results in

$$
\begin{aligned}
\dot{\tilde{\mathcal{R}}} &= -k_\omega\tilde{\mathcal{R}}(\tilde{\mathcal{R}} - \tilde{\mathcal{R}}^T) - \tilde{\mathcal{R}}[\mathcal{R}^C_B\mathbf{R}\tilde{\mathbf{b}}_\omega]_\times \\
\dot{\tilde{\mathbf{b}}}_\omega &= k_{b_\omega}{}^B_C\mathbf{R}\mathcal{R}^T[\tilde{\mathcal{R}} - \tilde{\mathcal{R}}^T]_\otimes
\end{aligned} \tag{11}
$$

Lemma 2 provides sufficient conditions for the boundedness of the estimation errors that exclude convergence to the equilibrium points satisfying $\|\tilde{\mathcal{R}} - \mathbf{I}\|^2 = 8$. Global asymptotic stability of the origin is precluded by topological limitations associated with those points [14].

Lemma 2: For any initial condition that verifies

$$
\frac{\|\tilde{\mathbf{b}}_\omega(t_0)\|^2}{8 - \|\tilde{\mathcal{R}}(t_0) - \mathbf{I}\|^2} < k_{b_\omega}, \tag{12}
$$

the estimation errors $\tilde{\mathbf{x}}_b = (\tilde{\mathcal{R}}, \tilde{\mathbf{b}}_\omega)$ are bounded and $\|\tilde{\mathcal{R}}(t) - \mathbf{I}\|^2 < 8$ for all $t \geq t_0$.

Exploiting the results derived for LTV systems in [15], Theorem 1 establishes the exponential convergence of the system (11) trajectories to the desired equilibrium point.

Theorem 1: Assume that $\boldsymbol{\omega}$, $\dot{\psi}$ and $\dot{\phi}$ are bounded. Then the attitude error and the bias estimation error converge exponentially fast to the equilibrium point $(\tilde{\mathcal{R}}, \tilde{\mathbf{b}}_\omega) = (\mathbf{I}, 0)$, for any initial condition satisfying (12).

Due to space constraints, the proofs of Lemma 2 and Theorem 1 are omitted. However, they can be obtained by adapting the proofs of Lemma 6 and Theorem 7 in [4].

IV. Camera Pan and Tilt Controller

In this section, we address the problem of keeping the features inside the image plane, exploring the camera's ability to describe pan and tilt angular motions. As stated in Problem 2, the strategy adopted to achieve this goal amounts to controlling the camera pan and tilt angular velocities $\dot{\psi}$ and $\dot{\phi}$, using directly the image measurements $\mathbf{y}_i$ and the angular velocity readings $\boldsymbol{\omega}_r$, so as to keep the image of the features' centroid at a close distance from the center of the image plane.

We resort to Lyapunov theory and consider the following candidate Lyapunov function

$$
W = \frac{1}{2}\mathbf{p}^T\Pi\mathbf{p} = \frac{1}{2}(p_x^2 + p_y^2), \tag{13}
$$

where $\mathbf{p} = [p_x\ p_y\ p_z]^T$ is the position of $\{L\}$ expressed in $\{C\}$ and $\Pi \in \mathbb{R}^{3\times3}$ is the x-y plane projection matrix. Using the expression for $\boldsymbol{\omega}$ given in (4), the camera position kinematics can be written as

$$
\begin{aligned}
\dot{\mathbf{p}} &= [\mathbf{p}]_\times\boldsymbol{\omega} - \mathbf{v} \\
&= [\mathbf{p}]_\times(\mathbf{R}_{\text{tilt}}^T\mathbf{R}_{\text{pan}}^T\boldsymbol{\omega}_B + \mathbf{R}_{\text{tilt}}^T[\dot{\phi}\ 0\ \dot{\psi}]^T) - \mathbf{v},
\end{aligned} \tag{14}
$$

where $\mathbf{v}$ is the camera linear velocity. Recall that by definition $\mathbf{p}$ coincides with the position of the features' centroid and its image is given by $\bar{\mathbf{y}}$. Therefore, by guaranteeing that the Lyapunov function W is decreasing, or equivalently $[p_x\ p_y]$ is approaching the origin, we can ensure that $\bar{\mathbf{y}}$ is approaching the center of the image plane. To simplify the notation and without loss of generality, assume from now on that $\mathbf{A} = \mathbf{I}$ so that $\bar{y}_x = p_x/p_z$ and $\bar{y}_y = p_y/p_z$.

Before proceeding to define the pan and tilt control law, we highlight the fact that $\bar{\mathbf{y}}$ can be easily obtained from the image measurements $\mathbf{y}_i$. By noting that the feature centroid lies at the intersection between the vectors $\mathbf{x}_3 - \mathbf{x}_1$ and $\mathbf{x}_4 - \mathbf{x}_2$ and the intersection between lines is clearly an image invariant, we can immediately conclude that $\bar{\mathbf{y}}$ coincides with the point at the intersection between $\mathbf{y}_3 - \mathbf{y}_1$ and $\mathbf{y}_4 - \mathbf{y}_2$.

Lemma 3: Let the camera position kinematics be described by (14) and assume that the rigid body and camera motions are such that $p_z > 0$ and $\cos\phi \neq 0$. Consider the control law for the camera pan and tilt angular velocities given by

$$\begin{bmatrix}\dot{\phi}\\ \dot{\psi}\end{bmatrix} = k_c \begin{bmatrix}0 & -1\\ \frac{1}{\cos\phi} & 0\end{bmatrix} \bar{\mathbf{y}} - \begin{bmatrix}1 & 0 & 0\\ 0 & -\tan\phi & 1\end{bmatrix} \mathbf{R}_{\text{pan}}^T \hat{\boldsymbol{\omega}}_B, \quad (15)$$

where $\hat{\boldsymbol{\omega}}_B = \boldsymbol{\omega}_r - \hat{\mathbf{b}}_\omega$ and $k_c > 0$. Then, the time derivative of the Lyapunov function W along the system trajectories satisfies

$$\dot{W} \leq -(k_c - \epsilon)W, \quad \forall \, \|\Pi\mathbf{p}\| \geq \frac{1}{\epsilon}\left(\|\Pi\mathbf{v}\| + p_z\|\tilde{\mathbf{b}}_w\|\right), \quad (16)$$

and $0 < \epsilon < k_c$.

Proof: Taking the time derivative of (13) and using the expressions for $\dot{\mathbf{p}}$ given in (14), we obtain

$$\begin{aligned}\dot{W} &= \mathbf{p}^T\Pi(p_z[\mathbf{e}_3]_\times \boldsymbol{\omega} - \mathbf{v})\\ &= p_z[p_y \;\; -p_x \;\; 0]\mathbf{R}_{\text{tilt}}^T(\mathbf{R}_{\text{pan}}^T\boldsymbol{\omega}_B + [\dot{\phi}\; 0\; \dot{\psi}]^T) - \mathbf{p}^T\Pi\mathbf{v}.\end{aligned}$$

Choosing $\dot{\phi}$ and $\dot{\psi}$ such that

$$\mathbf{R}_{\text{tilt}}^T(\mathbf{R}_{\text{pan}}^T\hat{\boldsymbol{\omega}}_B + [\dot{\phi}\; 0\; \dot{\psi}]^T) = -k_c[\bar{y}_y \;\; -\bar{y}_x \;\; \kappa]^T, \quad (17)$$

for some κ and noting that $\boldsymbol{\omega}_B = \hat{\boldsymbol{\omega}}_B - \tilde{\mathbf{b}}_w$ yields $\dot{W} = -k_c W - \mathbf{p}^T\Pi(\mathbf{v} + p_z[\mathbf{e}_3]_\times {}^C_B\mathbf{R}\tilde{\mathbf{b}}_w)$ and consequently (16) holds. Solving (17) for $\dot{\phi}$, $\dot{\psi}$, and κ, we obtain the control law (15). ∎

Remark 1: If we apply the control law (15) to the system with state $\Pi\mathbf{p} = [p_x \; p_y]^T$ and interpret $\mathbf{v}$ and $p_z\tilde{\mathbf{b}}_w$ as inputs, it follows from (16) that the system is exponentially input-to-state stable (ISS). As such, the distance between the image of the centroid $\bar{\mathbf{y}}$ and the origin is ultimately bounded by $\|\Pi\mathbf{v}/p_z\|$ and $\|\tilde{\mathbf{b}}_w\|$ and converges exponentially fast to that bound. Moreover, if $\Pi\mathbf{v}/p_z$ and $\tilde{\mathbf{b}}_w$ converge to zero so does $\bar{\mathbf{y}}$.

V. COMPUTATIONAL IMPLEMENTATION

In this section we describe the computational implementation of the attitude observer and camera pan and tilt controller proposed in Sections III and IV, respectively.

A. Discrete Time Algorithm

Several techniques can be adopted for discretization of nonlinear differential systems. The choice of algorithm depends on the specific problem, and stability and convergence are seldom guaranteed in general.

The discrete time algorithm is obtained by applying numerical integration methods to the observer continuous time dynamics. The integration method should guarantee that the discrete time implementation approximates conveniently the original continuous time observer. Classic Runge-Kutta methods cannot be correctly applied to rotation matrix dynamics since they are not able to preserve polynomial invariants, like the determinant, of degree higher than three [16, Theorem IV.3.3]. An alternative is to apply a method that preserves orthogonality, like a Lie group integrator.

The attitude observer dynamics is composed by differential equations (5) and (10), evolving in SO(3) and $\mathbb{R}^3$, respectively. The first is integrated resorting to geometric numerical integration methods namely, the Crouch-Grossman Method (CG) [9], the Munthe-Kaas Method (MK) [10], and the commutator-free Lie group Method (CF) [11]. The second is implemented in discrete time using a classical numerical integration technique.

The presented geometric numerical integration algorithms require the knowledge of the function $\hat{\boldsymbol{\omega}}(t)$ at instants between sampling times. In the present work, the unit is equipped with low cost inertial sensors and computational resources are limited, then $\hat{\boldsymbol{\omega}}$ is linearly interpolated in the interval $[(k-1)T,\; kT]$, where T is the sample period.

Due to the adopted interpolation, the use of integration methods with order higher than two does not improve the methods accuracy, hence we narrow our analysis to second order methods. The complexity required to implement each step of the second order CG and MK methods, is summarized in Table I, for the operations in SO(3), exponential map (Exp), inverse of the differential of the exponential map (Dexp^{-1}), and 3×3 matrix multiplication (mmult), as defined in [17]. The coefficients for these methods can be obtained in [16] and [17]. Note that there is no second order CF method and higher orders imply higher computational cost, hence it was not included in Table I. Due to its lower computational cost, the second order CG method is selected.

TABLE I

COMPLEXITY IN EACH STEP FOR SECOND ORDER CG AND MK METHODS.

operation	Exp	Dexp^{-1}	mmult
CG 2$^{\text{nd}}$ order	3	0	3
MK 2$^{\text{nd}}$ order	2	2	2

The discrete time implementation of equation (10) was obtained by using a second order *Adams-Moulton Method*, see [18] for further details. This selection was done based on arguments similar those used for (5). The resulting numerical integration algorithm can be summarized as

$$\begin{aligned}
\mathbf{s}_{\omega\; k-1} &= \sum_{i=1}^{5}(\hat{\mathcal{R}}_{k-1}^T {}^L\bar{\mathbf{X}}\mathbf{A}_X\mathbf{e}_i) \times (\mathbf{U}_{k-1}\mathbf{e}_i),\\
\hat{\boldsymbol{\omega}}^{(1)} &= \boldsymbol{\omega}_{r\; k-1} - \hat{\mathbf{b}}_{\omega\; k-1} - k_\omega \mathbf{s}_{\omega\; k-1},\\
Y &= \text{Exp}\left(-T[\hat{\boldsymbol{\omega}}^{(1)}]_\times\right)\hat{\mathcal{R}}_{k-1}^T,\\
\mathbf{s}_{\omega\; k}^Y &= \sum_{i=1}^{5}(Y^L\bar{\mathbf{X}}\mathbf{A}_X\mathbf{e}_i) \times (\mathbf{U}_k\mathbf{e}_i),\\
\hat{\mathbf{b}}_{\omega\; k} &= \hat{\mathbf{b}}_{\omega\; k-1} + \frac{Tk_{b_\omega}}{2}\left({}^B_C\mathbf{R}_k\mathbf{s}_{\omega\; k} + {}^B_C\mathbf{R}_{k-1}\mathbf{s}_{\omega\; k-1}\right)\\
\hat{\boldsymbol{\omega}}^{(2)} &= \boldsymbol{\omega}_{r\; k} - \hat{\mathbf{b}}_{\omega\; k} - k_\omega \mathbf{s}_{\omega\; k}^Y,\\
\mathcal{R}_k^T &= \text{Exp}\left(-\frac{T}{2}[\hat{\boldsymbol{\omega}}^{(2)}]_\times\right)\text{Exp}\left(-\frac{T}{2}[\hat{\boldsymbol{\omega}}^{(1)}]_\times\right)\mathcal{R}_{k-1}^T.
\end{aligned}$$

Fig. 3. Experimental setup.

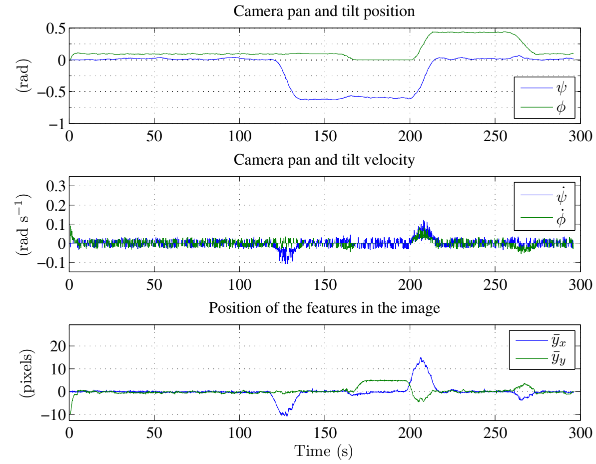

Fig. 4. Time evolution of the camera pan and tilt position and velocity and of the features' centroid in the image plane.

B. Multi-rate algorithm

The proposed attitude observer architecture includes the attitude algorithm, the camera pan and tilt controller, and the communication protocols with the camera and the rate gyros. Cameras typically have much lower sampling rates than inertial sensors. To accommodate the difference in sampling rates, we adopt a multi-rate strategy. While an image is being processed and the attitude feedback law cannot be applied, the attitude estimate $\hat{\mathcal{R}}$ is propagated by using solely the angular velocity readings $\boldsymbol{\omega}_r$. As soon as the image data is available, $\hat{\mathcal{R}}$ is recomputed using both $\boldsymbol{\omega}_r$ and the vector readings ${}^{C}\bar{\mathbf{X}}$. This algorithm increases the inter-sampling accuracy of the estimates, which may be of critical importance for control purposes.

VI. Experimental Setup

To assess the performance of the proposed observer, an experimental setup, comprising a MemSense nIMU and an AXIS 215 PTZ camera, was mounted on a Model 2103HT motion rate table, which enables the acquisition of ground truth data. Figure 3 shows the experimental setup together with the set of four colored circles that were used as visual features in the experiments.

The MemSense nIMU is a three-axis inertial measurement unit that incorporates a triad of rate gyros, a triad of accelerometers, and a triad of magnetometers. The rate gyros provide a dynamic range of ± 150 deg/s, with values of 0.36 deg/s and 0.95 deg/s for typical and maximum noise, respectively (1σ). The AXIS 215 PTZ is a network camera that can be controlled in pan, tilt, and zoom (± 170 deg pan range, 180 deg/s pan speed, 180 deg tilt range, and 140 deg/s tilt speed). The angular positions and speeds can be set with a resolution of 1 deg and 1 deg/s, respectively. The camera is interfaced via a local network and using the HTTP protocol.

The Model 2103HT from Ideal Aerosmith [12], is a three-axis motion rate table that provides precise angular position, rate, and acceleration for development and testing of inertial components and systems (position accuracy ± 0.0083 deg, rate accuracy $0.01\% \pm 0.0005$ deg/s).

VII. Experimental Results

This section describes the experimental results obtained for a typical trajectory generated by the motion rate table. The camera acquires images at 10 Hz and the rate gyros sampling rate is 150 Hz.

The rate gyros measurement noise is characterized by a standard deviation of 0.0105 rad/s, 0.0100 rad/s, and 0.0105 rad/s (1σ), for the x, y, and z axis, respectively. Regarding the visual features, the measurement noise exhibited a standard deviation of 0.7 pixels. The measurement noise characterization can be used to adequately select the observer gains. This is accomplished by running the observer in simulation using the same experimentally acquired measurement noise and searching for the minimum error over a discrete array of values for the gains k_ω $(10^{-1}, 10^{-0.5}, 10^{0}, 10^{0.5}, 10^{1})$, k_{b_ω} $(10^{-2}, 10^{-1}, 10^{0}, 10^{1})$. The minimum quadratic error was obtained for the pair $k_\omega = 10^0$, $k_{b_\omega} = 10^{-1}$.

Figure 4 shows the time evolution of the camera pan and tilt position and velocity, and the time evolution of the features' centroid in the image plane. Despite the reasonable range of movements of the trajectory, the features remain visible throughout the experiment due to the compensation provided by the camera pan and tilt controller.

Figure 5 shows the estimation results provided by the method proposed in this paper. To illustrate the advantages of the proposed algorithm, we computed at each instant the solution to Wahba's problem and used it as an alternative attitude estimate for the same experiment. As opposed to the dynamic observer proposed in this paper, the estimation method based on Wahba's problem neglects all knowledge of previous estimates and relies solely on the vector readings extracted from the image measurements. Figure 6 shows the estimation errors produced by both methods. The proposed solution display a significant increase in accuracy. The standard deviation obtained with the proposed solution are 0.0034 rad, 0.0083 rad, and 0.0141 rad, for roll, pitch and yaw, respectively; and standard deviation obtained with the Wahba's solution are 0.0091 rad, 0.0208 rad, and 0.0296 rad for roll, pitch and yaw, respectively.

Figure 7 shows the time evolution of the angular rate bias estimates. A transient occur during the first 50 seconds as result of the initial estimation errors. Although the rate gyros

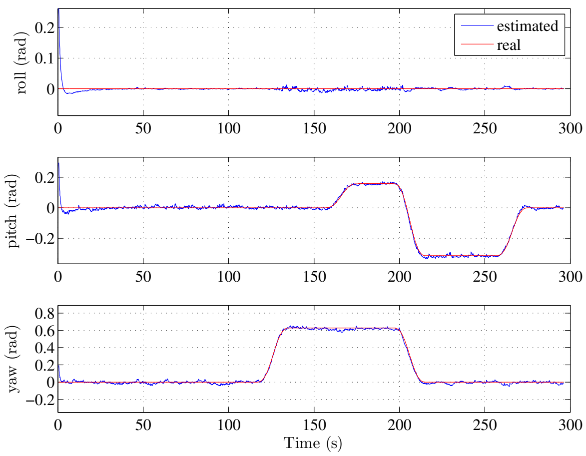

Fig. 5. Attitude estimation using the proposed algorithm.

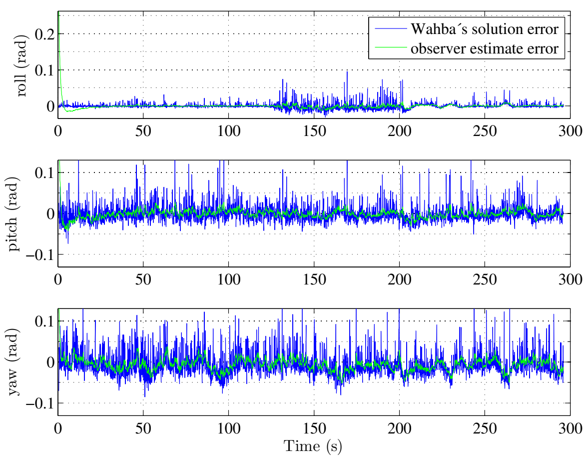

Fig. 6. Error of the attitude determination using the solution for the Wahba's problem and the proposed algorithm.

estimates never reach a steady state due to the noise present in the measurements, after this period, they are restrained to tight intervals.

VIII. CONCLUSIONS

This paper addressed the problem of estimating the attitude of a rigid body equipped with a triad of rate gyros and a pan and tilt camera. An exponential input-to-state stable pan and tilt control law that enforces feature visibility was introduced. A multi-rate implementation of the nonlinear attitude observer that uses recent results in geometric numeric integration was proposed and experimentally tested. A griding technique was used to obtain suitable feedback gains for the observer. The high level of performance attained by the proposed solution was experimentally demonstrated resorting a three-axis motion rate table.

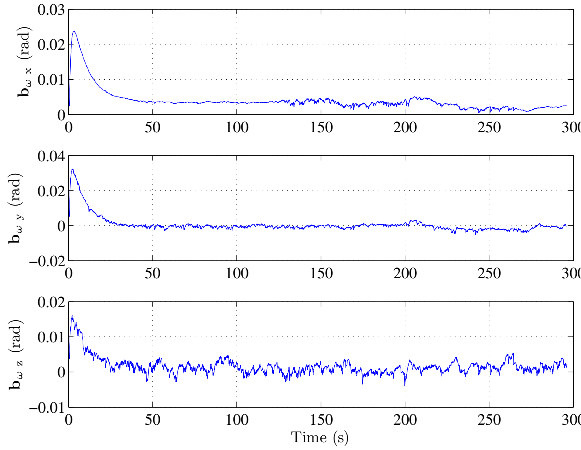

Fig. 7. Angular rate bias estimation.

REFERENCES

[1] N. Cowan, J. Weingarten, and D. Koditschek, "Visual servoing via navigation functions," *IEEE Transactions on Robotics and Automation*, vol. 18, no. 4, pp. 521–533, 2002.

[2] E. Malis and F. Chaumette, "Theoretical improvements in the stability analysis of a new class of model-free visual servoing methods," *IEEE Transactions on Robotics and Automation*, vol. 18, no. 2, pp. 176–186, 2002.

[3] A. P. Aguiar and J. Hespanha, "Minimum-energy state estimation for systems with perspective outputs," *IEEE Transactions on Automatic Control*, vol. 51, no. 2, pp. 226–241, 2006.

[4] J. F. Vasconcelos, R. Cunha, C. Silvestre, and P. Oliveira, "Landmark based nonlinear observer for rigid body attitude and position estimation," in *17th IFAC World Congress*, South Korea, Seoul, Jul. 2008.

[5] R. Mahony, T. Hamel, and J. M. Pflimlin, "Nonlinear complementary filters on the special orthogonal group," *IEEE Transactions on Automatic Control*, vol. 53, no. 5, pp. 1203–1218, Jun. 2008.

[6] N. Chaturvedi and N. McClamroch, "Almost global attitude stabilization of an orbiting satellite including gravity gradient and control saturation effects," in *American Control Conference*, Minnesota, USA, Jun. 2006.

[7] D. Fragopoulos and M. Innocenti, "Stability considerations in quaternion attitude control using discontinuous Lyapunov functions," *IEEE Proceedings on Control Theory and Applications*, vol. 151, no. 3, pp. 253– 258, May 2004.

[8] D. E. Koditschek, "The Application of Total Energy as a Lyapunov Function for Mechanical Control Systems," *Control Theory and Multibody Systems*, vol. 97, pp. 131–151, 1989.

[9] P. E. Crouch and R. Grossman, "Numerical integration of ordinary differential equations on manifolds," *Journal of Nonlinear Science*, vol. 3, pp. 1–33, 1993.

[10] H. Z. Munthe-Kaas, "Runge-Kutta methods on Lie groups," *BIT Numerical Mathematics*, vol. 38, no. 1, pp. 92–11, 1998.

[11] E. Celledoni, A. Marthinsen, and B. Owren, "Commutator-free Lie group methods," *Future Generation Computer Systems*, vol. 19, no. 3, pp. 341–352, Apr. 2003.

[12] I. Ideal Aerosmith. (2006) 2103ht multi-axis table data sheet, rev c. [Online]. Available: http://www.ideal-aerosmith.com/

[13] R. Cunha, "Advanced motion control for autonomous air vehicles," Ph.D. dissertation, Instituto Superior Técnico, Lisbon, 2007.

[14] S. P. Bhat and D. S. Bernstein, "A topological obstruction to continuous global stabilization of rotational motion and the unwinding phenomenon," *Systems and Control Letters*, vol. 39, no. 1, pp. 63–70, Jan. 2000.

[15] A. Loría and E. Panteley, "Uniform exponential stability of linear time-varying systems: revisited," *Systems and Control Letters*, vol. 47, no. 1, pp. 13–24, Sep. 2002.

[16] E. Hairer, C. Lubich, and G. Wanner, *Geometric Numerical Integration, Structure-Preserving Algorithms for Ordinary Differential Equations*, 2nd ed., ser. Springer Series in Computational Mathematics. Springer, 2006, vol. 31.

[17] J. Park and W.-K. Chung, "Geometric integration on Euclidean group with application to articulated multibody systems," *IEEE Transactions on Robotics*, vol. 21, no. 5, pp. 850–863, Oct. 2005.

[18] R. Burden and J. Faires, *Numerical Analysis*. Boston: PWS-KENT Publishing Company, 1993.